Supporting Information for

Prediction of intrinsic room-temperature ferromagnetism in two-dimensional $CrInX_2$ (X = S, Se, Te) monolayers

Yunfei Zhang,[a] Shuo Zhang,[a] Minghao Jia,[b] Tian Wang,[b] Lixiu Guan,[b,*] and Junguang Tao[a,*]

[a]School of Materials Science and Engineering, Hebei University of Technology, Tianjin 300132, China

[b]School of Sciences, Hebei University of Technology, Tianjin 300401, China

The structure design of $CrInX_2$ (X = S, Se, Te) with the evolutionary algorithm:

Since the experimental reporting of the two-dimensional (2D) magnetic layered materials CrI_3 and $Cr_2Ge_2Te_6$ in 2017, the investigation on 2D magnetic materials has stirred great enthusiasm among the community. Unfortunately, only a few 2D magnetic materials can be experimentally synthesized and their T_c are fairly below the room temperature. Although methods such as mechanical peeling and chemical vapor deposition (CVD) have become relatively mature, preparing high-quality monolayer van der Waals (vdW) materials is still challenging. In addition, since the possible 2D magnetic materials have multiple structures and their experimental synthesis usually consumes a lot of time, resulting in a waste of resources and research delays. Therefore, rational theoretical designs and predictions are of time-efficiency for accelerating the

screening of 2D magnetic candidate materials with desired characteristics, which do not require expending efforts on the synthesis of relevant materials.

To achieve this goal, several structural prediction methods have been developed based on the exploration of potential energy surface (PSE), including data mining, minima hopping, genetic algorithm and energy minimization, basin-hopping, and particle-swarm optimization (PSO). Among them, PSO, as a random global optimization method, was first proposed by Kennedy and Eberhart in the 1990s.[1, 2] Subsequently, Wang and Ma *et. al.*[3] combined the advantages of PSO method and other key technologies to develop the CALYPSO method. CALYPSO software can be used to predict the crystal structure of materials under given chemical composition and external conditions.

So far, the CALYPSO method has successfully predicted many new materials, especially under high pressure conditions, and these prediction results have been experimentally verified with significant success.[4-6] In the CALYPSO method, the developed 2D structure searching module can efficiently and accurately predict a few layer structure. Overall, the PSO algorithm used for crystal prediction in CALYPSO software consists of four main processes: (1) generation of random structures, (2) structural optimization, (3) identification of minimum energy values, and (4) generation of new structures. In order to improve the efficiency of

structural design and prediction while reducing computational costs, CALYPSO also integrates various key technologies, including structural evolution, structural characterization techniques, symmetric constraints, and local structural optimization.

In this work, we successfully predicted the low-energy structure of 2D single-layer $CrInX_2$ using the CALYPSO software package and an evolutionary algorithm based on the PSO method. In the PSO simulation, we set a population size of 30 and an iteration number of 50, which generated 1500 structures and sorted by their relative energy. As a start, the $CrInX_2$ molecule is placed in the *x*-*y* plane and designed as a layered structure with wrinkles, while the thickness of the vacuum layer is set to 30 Å. In the first generation, the structure was automatically generated as a random structure based on the requirements for atomic type, number, and ratio in the input file. Only 60% of the structure was passed on to the next generation to ensure structural diversity.

Additional electronic structures information for $CrInX_2$ (X = S, Se, Te)

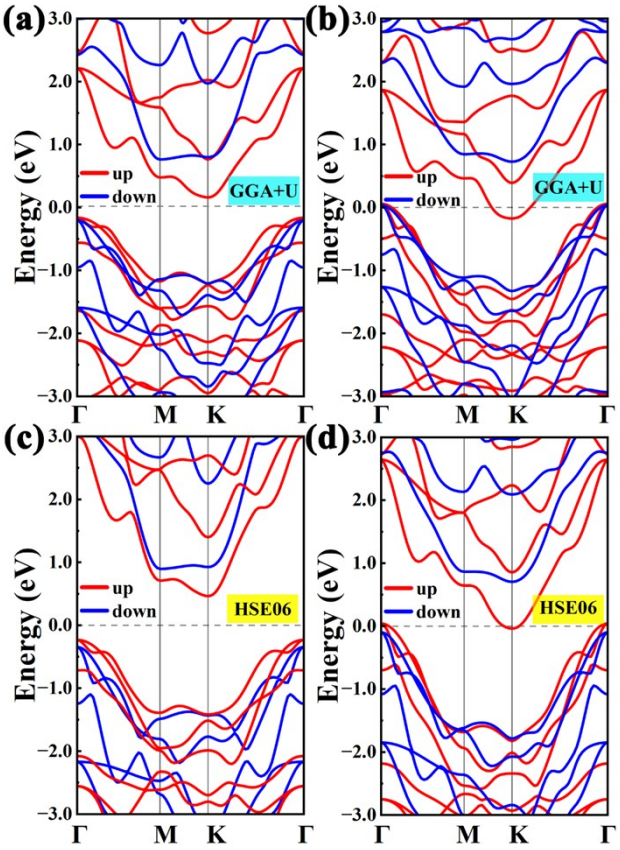

Figure S1. Band structures of $CrInSe_2$ and $CrInTe_2$ at GGA+U (a, b) level and HSE06 level (c, d). The red and blue curves represent the spin-up and spin-down bands, respectively.

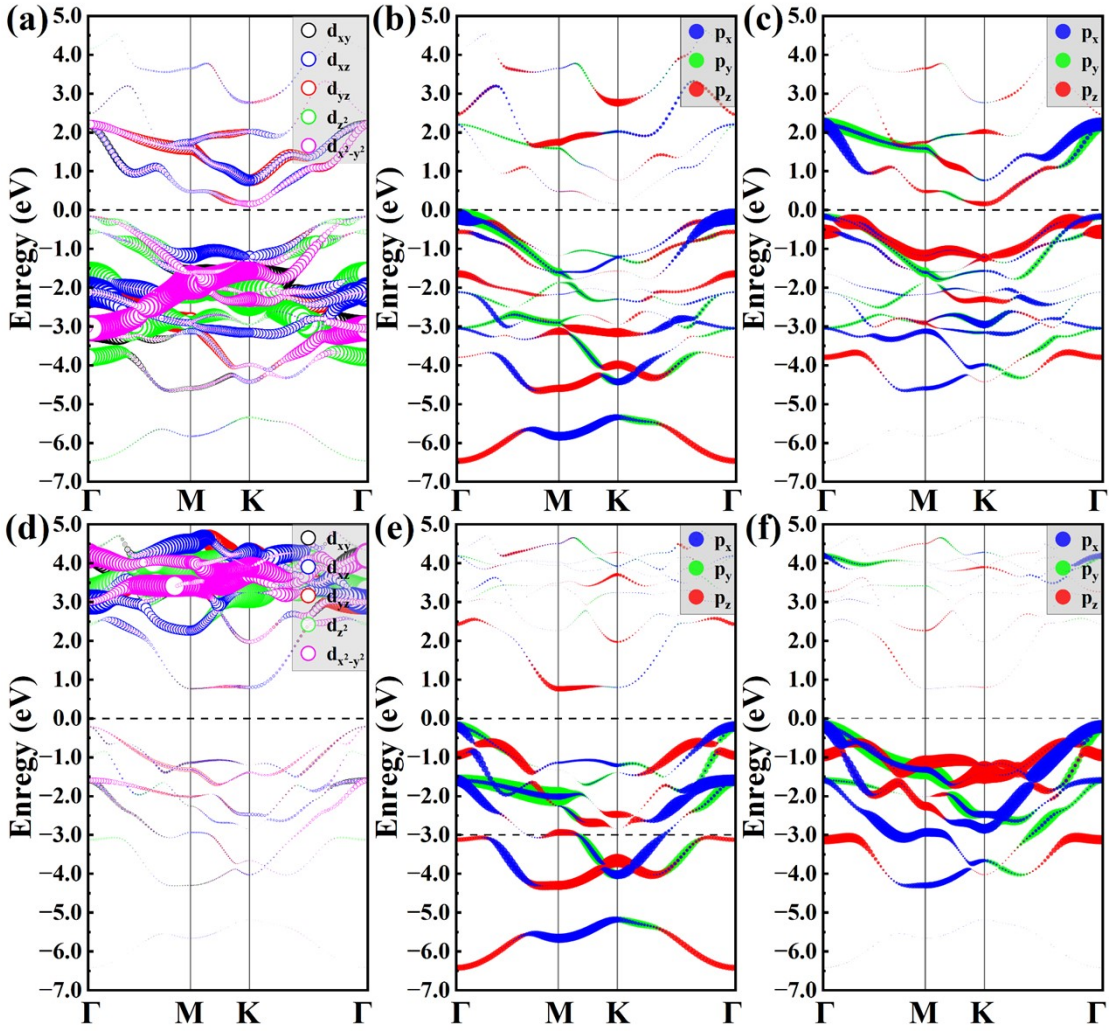

Figure S2. Orbital projected band structure of $CrInSe_2$ monolayer. (a) spin-up and (d) spin-down channels for Cr 3*d* orbitals; (b) spin-up and (e) spin-down channels for S_1 *p* orbital; (c) spin-up and (f) spin-down channels for S_2 *p* orbital.

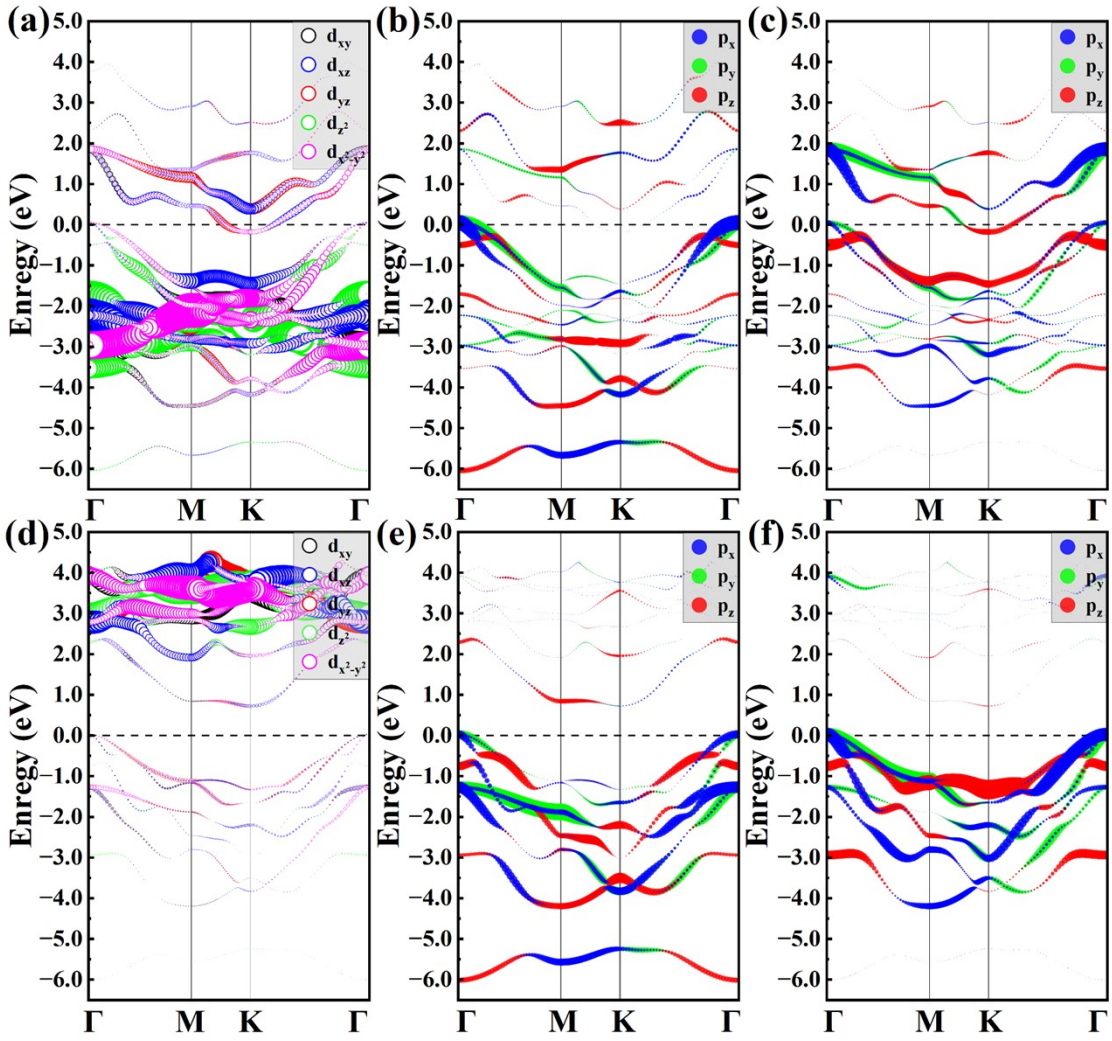

Figure S3. Orbital projected band structure of $CrInTe_2$ monolayer. (a) spin-up and (d) spin-down channels for Cr 3*d* orbitals; (b) spin-up and (e) spin-down channels for S_1 *p* orbital; (c) spin-up and (f) spin-down channels for S_2 *p* orbital.

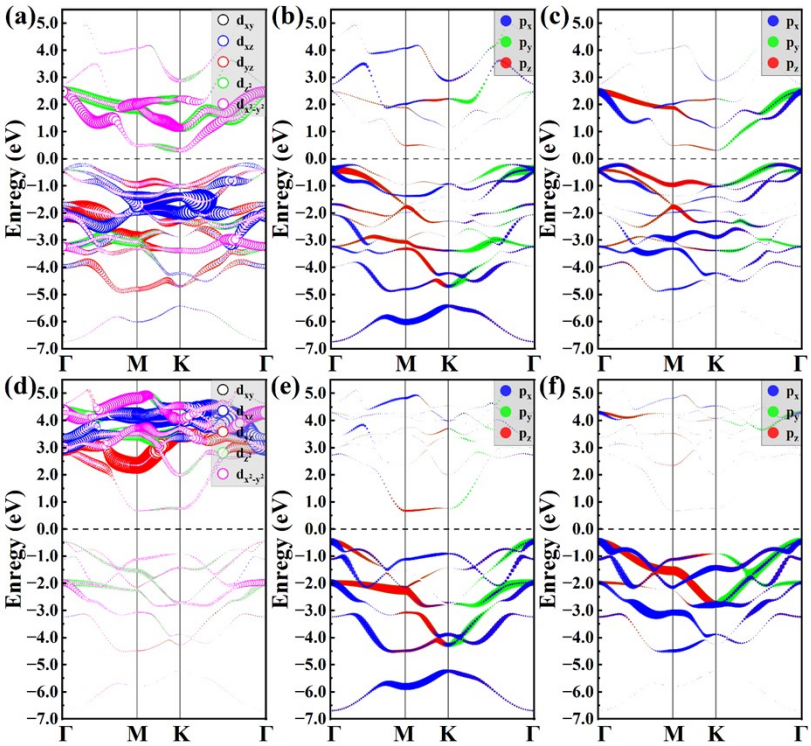

Figure S4. Orbital projected energy band structure of the $CrInS_2$ monolayer in the local coordinate system. (a) spin-up and (d) spin-down channels for Cr 3*d* orbitals; (b) spin-up and (e) spin-down channels for S_1 *p* orbital; (c) spin-up and (f) spin-down channels for S_2 *p* orbital.

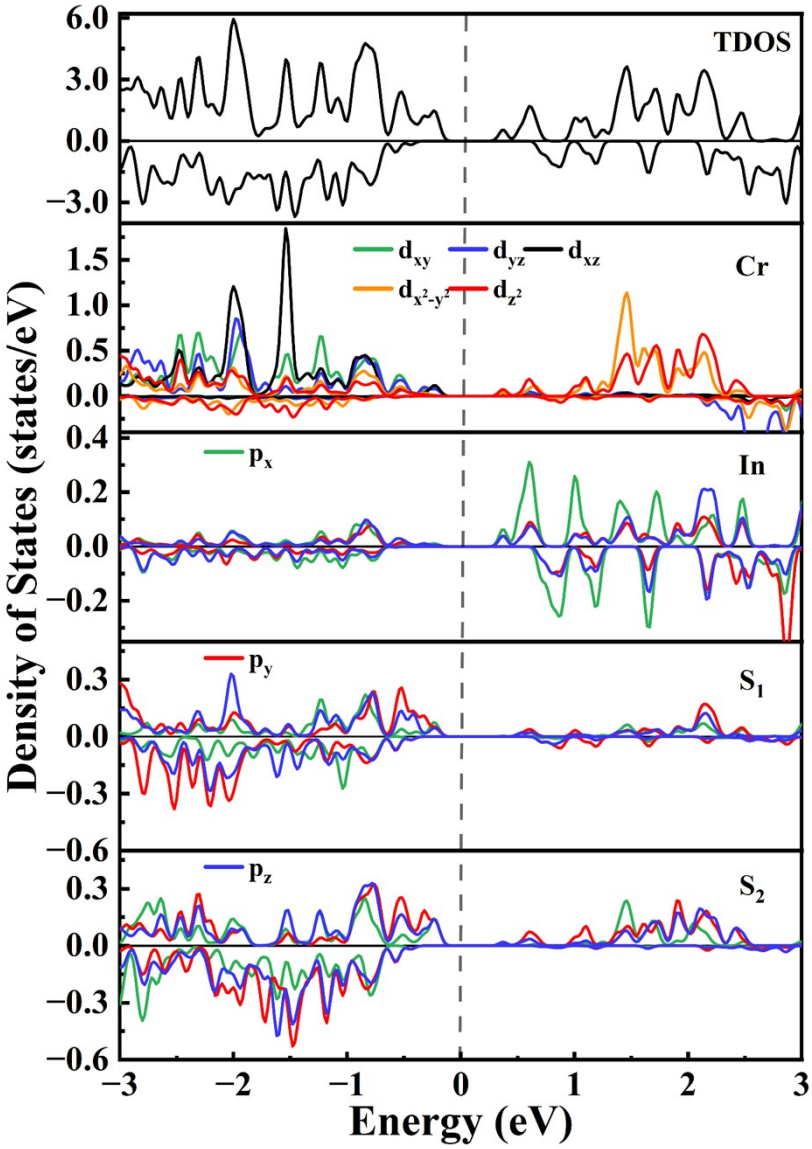

Figure S5. Total density of state (TDOS) and projected density of state (PDOS) of $CrInS_2$ in the local coordinate system.

Electronic structure analysis of $CrInSe_2$ and $CrInTe_2$ monolayers and electronic structure analysis of $CrInS_2$ in local coordinate system:

In the main text, we have mainly analyzed the electronic structure of monolayer $CrInS_2$. Here, we will further analyze the electronic structures

of $CrInSe_2$ and $CrInTe_2$. As shown in Fig. 3 and Figs. S2-S3, the band structure characteristics of the three different materials share great similarity. In addition, their band structures also exhibit a gradual change as the anion atoms go from S to Te. For instance, with the increase of atomic number, the energies of X p_x and p_y orbitals gradually rise up to eventually cross the Fermi level (E_F). For Cr, its $d_{x^2-y^2}$ orbital, which constitutes the CBM, gradually shifts downwards. All of these behaviors result in a gradual decrease in the band gaps of the system and ultimately render $CrInTe_2$ a metallic ground state. On the other hand, unlike $CrInS_2$, the valance band maximum (VBM) for $CrInSe_2$ is located at *Γ* point and mainly composed of Cr d_{z^2} orbital and Se p_x and p_y orbitals. However, the location of its conduction band minimum (CBM) remains as same as that of $CrInS_2$ at *K* point.

Further analysis was conducted on the projected band structure and TDOS for a monolayer of $CrInS_2$ in the local coordinate system, as depicted in Figs. S4 and S5. The VBM is primarily constituted by the t_{2g} orbitals of Cr atoms and the *p* orbitals of the outer S_2 atoms, with a partial contribution from the *p* orbitals of the inner S_1 atoms. On the other hand, the CBM mainly originates from the e_g orbitals of Cr and the *p* orbitals of In atoms, complemented by contributions from the p_y and p_z orbitals of S_2 atoms. Notably, a more pronounced hybridization between the Cr t_{2g} orbitals and the S_2 *p* orbitals is observed near the VBM.

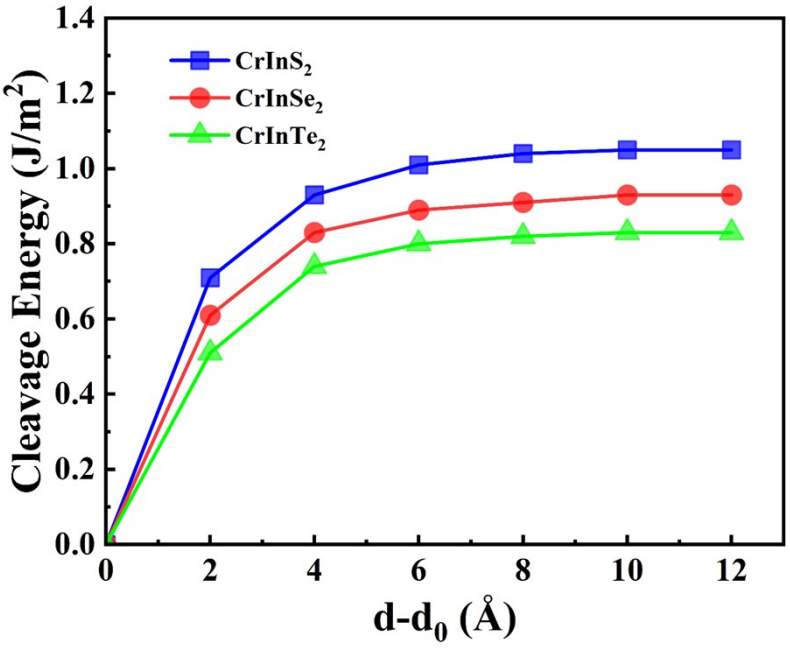

Figure S6. Cleavage energies of $CrInS_2$, $CrInSe_2$ and $CrInTe_2$, calculated by expanding the interlayer distance between the remaining portion of the 4-layer slab and the top layer.

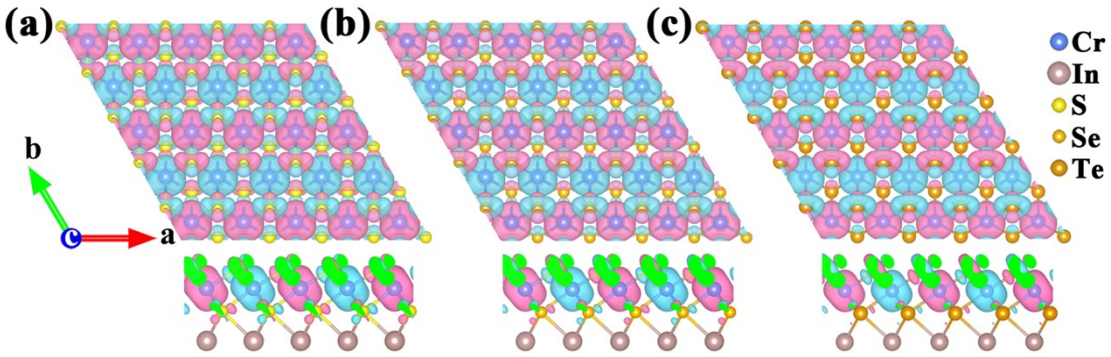

Figure S7. Spin density distributions of (a) $CrInS_2$, (b) $CrInSe_2$ and (c) $CrInTe_2$ with an isosurfaces of 0.003 e Å^{-3}. The pink-violet and cyan contours represent spin-up and spin-down polarization. Blue, brown, yellow, orange and brown balls represent Cr, In, S, Se and Te atoms, respectively.

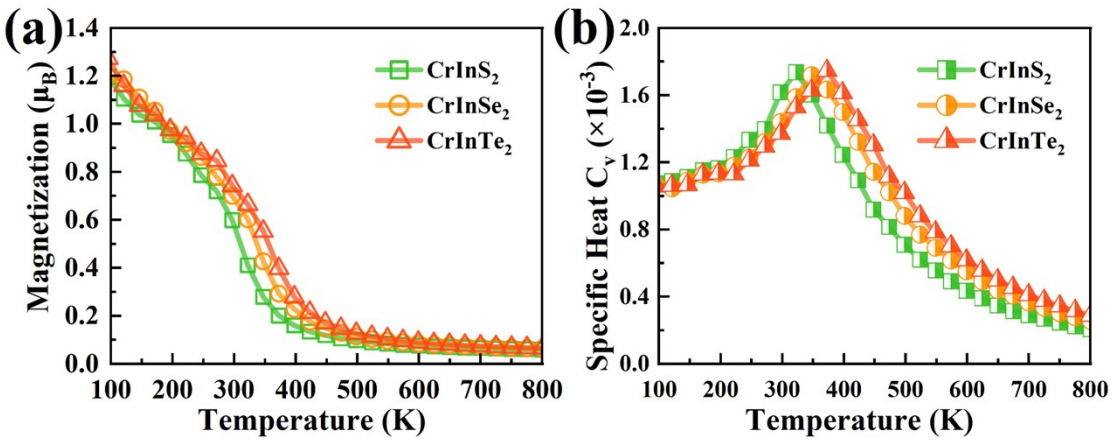

Figure S8. Monte Carlo simulation results of (a) mean magnetic moment and (b) specific heat as a function of temperature for $CrInS_2$, $CrInSe_2$ and $CrInTe_2$, considering overall exchange.

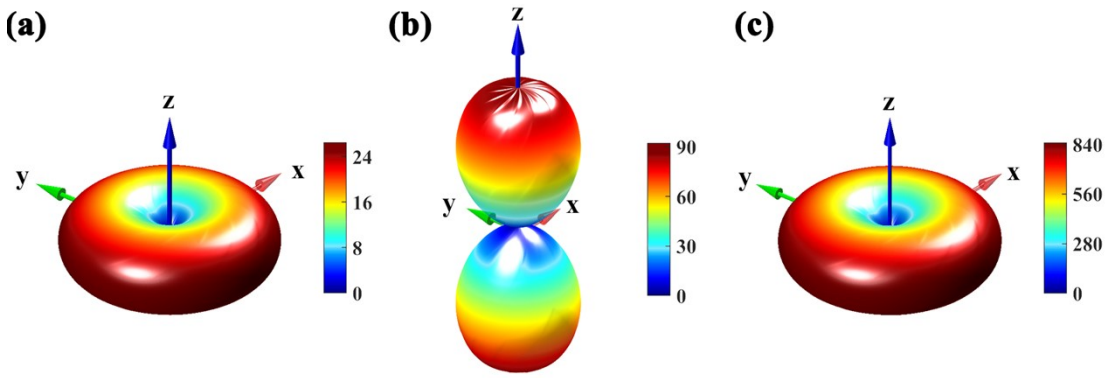

Figure S9. Three-dimensional view of the MAEs of (a) $CrInS_2$, (b) $CrInSe_2$ and (c) $CrInTe_2$. The transition from red to blue represents the change from easy to hard magnetization.

TABLES

Table S1. The energy and energy difference ΔE between the initial structure (X-Cr-In-X) and the predicted structure (X_2-Cr-X_1-In) using evolutionary algorithms.

System	Energy (eV/unit cell)		ΔE (meV/unit cell)
	X-Cr-In-X	X_2-Cr-X_1-In	
$CrInS_2$	-21.04	-20.21	831.27
$CrInSe_2$	-19.54	-18.81	729.86
$CrInTe_2$	-17.85	-17.25	604.75

Table S2. The Bader charge analysis of $CrInX_2$ monolayers.

System	Cr (electron)	In (electron)	X_1 (electron)	X_2 (electron)
$CrInS_2$	-1.2282	-0.4759	+0.9942	+0.7099
$CrInSe_2$	-1.0673	-0.4264	+0.8817	+0.6121
$CrInTe_2$	-0.8265	-0.3476	+0.7110	+0.4631

Table S3. Crystal field splitting energy and spin-up and spin-down orbital potential energies of $CrInS_2$ monolayer in the octahedral local coordinate system.

System	Spin direction	Δ_O (eV)	e_g (eV)		t_{2g} (eV)		
			d_{z^2}	$d_{x^2-y^2}$	d_{xy}	d_{yz}	d_{xz}
$CrInS_2$	up	0.94	0.07	0.08	-2.17	-2.17	-2.17
	down		3.00	2.99	3.26	3.26	3.27

References:

1. J. Kennedy, R.C. Eberhart, A discrete binary version of the particle swarm algorithm, IEEE, 1997, pp. 4104-4108.
2. Eberhart, S. Yuhui, Particle swarm optimization: developments, applications and resources, IEEE, Piscataway, NJ, USA, 2001, pp. 81-86.
3. Y. Wang, J. Lv, L. Zhu, Y. Ma, *Comput. Phys. Commun.*, 2012**, 183**, 2063-2070.
4. C. Tang, L. Zhang, S. Sanvito, A. Du, *J. Am. Chem. Soc.*, 2023**, 145**, 2485-2491.
5. D. Chen, Y. Wang, R. Dronskowski, *J. Am. Chem. Soc.*, 2023**, 145**, 6986-6993.
6. X. Hu, R.-W. Zhang, D.-S. Ma, Z. Cai, D. Geng, Z. Sun, Q. Zhao, J. Gao, P. Cheng, L. Chen, K. Wu, Y. Yao, B. Feng, *Nano Lett.*, 2023**, 23**, 5610-5616.